CHINESE OPTICS LETTERS

Vol. 23, No. 1 | January 2025

Light-activated film diffractive optical elements enable diversified optical field modulation

Ning Shen (沈 柠)[1,2], Honglong Hu (胡宏龙)[1,3], Zhaoyi Wang (王兆亿)[1], Yuxing Zhan (占宇星)[1,2], Conglong Yuan (袁丛龙)[1,3*], and Zhigang Zheng (郑致刚)[1,2]

[1] School of Physics, East China University of Science and Technology, Shanghai 200237, China

[2] School of Materials Science and Engineering, East China University of Science and Technology, Shanghai 200237, China

[3] School of Chemistry and Molecular Engineering, East China University of Science and Technology, Shanghai 200237, China

*Corresponding author: conglongyuan@ecust.edu.cn

Received June 7, 2024 | Accepted July 29, 2024 | Posted Online January 27, 2025

We propose a promising method to develop flexible, compact, and tunable light-activated film diffractive optical elements (FDOEs) with exceptional diffraction efficiency, by integrating liquid crystal (LC) geometric phase-based diffractive optical elements (DOEs) with a specifically designed light-activated LC polymer (LCP) film. Arbitrary film bending induced by UV/Vis irradiation is realized through precise mesogens arrangement within the LCP film, enabling 1D and 2D beam steering, as well as dynamic and reversible switching between structured and Gaussian lights after cooperating with the DOE design. Furthermore, remarkable fatigue resistance, solvent resistance, and thermal stability are demonstrated, providing a solid material platform for advanced optical applications.

Keywords: diffractive optical elements; liquid crystal polymer; light-activated film; optical field modulation.
DOI: 10.3788/COL202523.011602

1. Introduction

Over the past few decades, there has been a remarkable surge in technological advancements rooted in optoelectronics and photonics, spanning optical communication, beam manipulation, and light-field displays[1–4]. These developments have fundamentally revolutionized the transmission, manipulation, and visualization of light[5–7]. The foundational components of these technologies include refractive, diffraction, and optical fiber components[1,8]. In particular, the diffractive optical elements (DOEs)[7,9,10] have garnered significant attention due to their promising potential in catalyzing and enhancing various applications within the optical domain, such as spectral optimization[11], fiber coupling[12], beam shaping[13], and laser coherent combination[14]. Therein, by virtue of the unique combination between relatively large birefringence, controllable optical axis arrangements, and stimuli-directing optical properties of liquid crystals (LCs), LC geometric phase-based DOEs have obtained widespread favor across diverse fields such as augmented reality/virtual reality (AR/VR) display, imaging, planar optics, and multidimensional optical field modulation[15–18]. However, traditional LC DOEs are predominantly manufactured on rigid substrates, such as glass, facing significant limitations in flexibility, compactness, and integration capability. Hence, developing freestanding DOEs with tunable properties remains a challenging yet indispensable endeavor.

Liquid crystal polymers (LCPs), comprising a combination of the elasticity inherent in polymer networks and the ordered arrangement of LCs, exhibit a plethora of unique properties, such as elasticity, self-assembly, anisotropy, stimulus-responsiveness, and molecular-cooperation[19–21]. Therefore, LCPs become an ideal candidate for the development of flexible, lightweight, and stable thin-film DOEs, such as grating, q-plate, and fork grating[6,22–25]. From another perspective, positioned as quintessential stimulus-responsive polymers, LCPs have a wide range of applications in areas such as artificial muscles[26–28], soft robotics[29–33], smart wearables[34], and biomedicine[35,36], owing to their capacity for reversible actuation under diverse external stimuli, spanning heat, light, electric fields, mechanical force, and humidity[20,37–41]. Hence, the development of tunable film DOEs based on LCPs presents significant potential and holds the promise of advancing the integration and miniaturization of optical systems to new heights. Unfortunately, a conundrum arises as the superior optical effects of the film DOEs often conflict with the desired tunable properties, which is primarily caused by the inherent stability of the polymer network and the internal mechanism of the reversible actuation that the alignment of the LC mesogens in the LCP from order to disorder[38]. This obstacle significantly hindered the development of optical systems toward integration, weight reduction, and miniaturization. Thus, there exists an imperative mandate to

chart a new course, devising innovative strategies to realize compact, flexible, and tunable film DOEs with excellent optical effects.

Herein, we introduce a promising solution for fabricating flexible, compact, and tunable film diffractive optical elements (FDOEs). This approach involves the integration of LC geometry phase-based DOEs with specifically designed light-activated LCP films, which can undergo photodeformation via the trans-to-cis photoisomerization of azobenzene derivatives. Through the meticulous design of both the DOEs and the arrangement of mesogens in the light-activated LCP film, the proposed FDOEs enable not only 1D and 2D continuous and reversible beam steering but also dynamic switching between structured and Gaussian lights, while maintaining high diffraction efficiency. For example, integrating a thin-film polarization grating (PG) and a light-activated film with different mesogens arrangement facilitates the dynamic beam steering, resulting in the migration in the 1D direction and the rotation in the 2D plane of ±1st order diffraction spots under UV/Vis light irradiation. Additionally, a light-activated film fork polarization grating (FPG) is achieved, enabling the ±1st diffracted order to be reversibly switched between vortex light and Gaussian light. Similarly, the light-activated film Airy mask and q-plate demonstrate reversible switching between Airy beam/vortex light and Gaussian light, verifying the universality of the method. Noteworthy, a wide spectral operating band of incident light is achieved by wittily designing the light-activated film, further proving the practicability of the light-activated FDOEs. Consequently, the proposed light-activated FDOEs introduce a new paradigm, which provides more possibilities for flexibility, compact, and tunable DOEs that meet the needs of diversified application scenarios and advance the integration, weight reduction, and miniaturization of optical systems.

2. Results and Discussion

The light-activated FDOEs are fabricated by stacking a high-efficiency LC geometry phase-based DOEs layer and an azobenzene derivate-based light-activated LCP film. The preparation processes of the DOEs, the light-activated LCP film, and the light-activated FDOEs are described in detail in Fig. S1 and Sec. S1 (Supplementary Information). Therein, the high-efficiency and excellent optical performance of the LC geometry phase-based DOEs are attributed to digital micro-mirror device (DMD)-based LC photoalignment technology, film spin-coating technique, and the high optical transmittance of LCP material. Additionally, the light-activated LCP film can be engineered to exhibit controllable deformation directions under UV irradiation by designing the mesogens arrangement. This is due to the reversible trans-to-cis photoisomerization of the azobenzene derivates, which decreases the nematic ordering in the LCP film and then induces contraction along the alignment direction and expansion perpendicular to it. Noteworthy, to overcome the limitations imposed by azobenzene derivatives on the incident light wavelength, the light-activated LCP film is partitioned into two segments: a light-transmitting part that transmits the diffracted light of the DOE and a photodeformable section that alters the position of the DOE relative to the incident light. Noteworthy, the area of the light-transmitting part should adequately cover the DOE microstructure without affecting the photodeformation of the light-activated LCP film (Fig. S3, Supplementary Information).

Based on this design, the ±1st order diffraction spots generated by a PG migrate laterally in the 1D direction, i.e., the diffraction angle changes, as the change in the incident angle of the probe light when the light-activated FDOE bends along the x-axis under UV irradiation [Fig. 1(a)]. Similarly, configuring the mesogens arrangement of the light-activated LCP film along the diagonal [the white dashed box in Fig. 1(b)] results in the light-activated FDOE bending along the diagonal under UV irradiation [the black dashed box in Fig. 1(b)]. Consequently, the microstructure of the optical element distorts in a 2D plane relative to the probe light, leading to the rotation of the ±1st order diffraction spots in the 2D plane, as displayed in Fig. 1(b). Furthermore, both the 1D and 2D beam steering can be reversibly recovered by irradiating visible light. Thus, a light-activated FDOE is achieved, demonstrating the capability for 1D and 2D dynamic, continuous, and reversible beam steering.

As illustrated in Fig. 2(a), the bending along the x-axis occurs in light-activated FDOEs after irradiating UV light, with subsequent recovery under the visible light. Here, a 20 μm-period thin-film PG, whose phase distribution and polarization optical microscopy (POM) texture are depicted in Fig. 2(b), is employed as an LC geometry phase-based DOE to produce the light-activated FDOE by combining with the light-activated LCP film. The fabricated PG with continuously space-variant LC mesogens distribution demonstrates outstanding optical performance across various polarization states and wavelengths of incident lights, under the corresponding half-wave condition (Fig. S4, Supplementary Information). The light-activated film PG exhibits bending along the x-axis, resulting in the lateral migration of the ±1st order diffraction spots upon UV light irradiation, changing the diffraction angle. This migration of the diffraction spots is fully reversible upon visible light irradiation, showcasing the superior capability of 1D dynamic, continuous, and reversible beam steering [Figs. 2(c)–2(e), Movie S1, Supplementary Information]. The tunable diffraction angle range of 0.7° can be further extended by reducing the PG period and expanding the PG area. Interestingly, the light-activated film PG exhibits versatility across a wide spectral range of incident light, benefiting from the unique design of the light-activated LCP film, as shown in Figs. 2(c) and 2(e). This further demonstrates the broad applicability and potential of the light-activated film PG. Furthermore, it maintains high diffraction efficiency during beam steering, with an initial diffraction efficiency of 96.6% and a minimum diffraction efficiency of 84.1% [Fig. 2(f)].

In addition, the dynamic and continuous 2D beam steering is realized. As illustrated in Fig. 3(a), by designing the arrangement of the LC mesogens in the light-activated LCP film along the

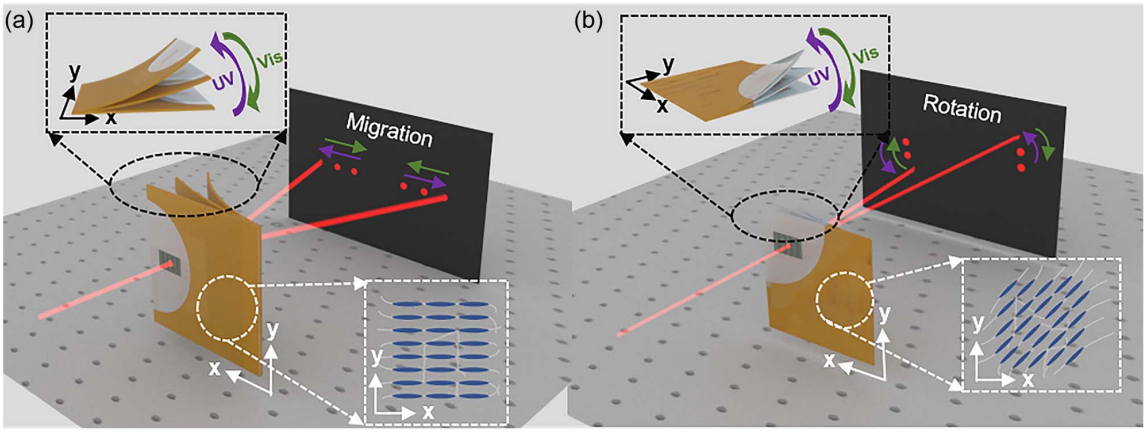

Fig. 1. Schematic diagram of the light-activated FDOEs. (a) Diagram of the light-activated FDOE with 1D beam steering. The mesogen arrangement in the light-activated LCP film aligns along the *x*-axis (white dashed box), causing UV/Vis-induced film deformation of the FDOE (black dashed box) along the same axis. Consequently, the ±1st order diffraction spots migrate in the 1D direction as the FDOE bends. (b) Diagram of the light-activated FDOE with 2D beam steering. The mesogen arrangement in the light-activated LCP film aligns along the diagonal (white dashed box), leading to UV/Vis-induced film deformation of the FDOE (black dashed box) along the same diagonal. Consequently, the ±1st order diffraction spots rotate in the 2D plane as the FDOE bends.

diagonal direction, the FDOE can bend along the same direction under UV irradiation. Subsequently, the incident light transitions from being vertically incident on a rectangular PG to being obliquely incident in 2D plane, which is equivalent to the incident light being vertically incident on a parallelogram PG (Fig. S5, Supplementary Information), leading to the rotational movement of the ±1st order diffraction spots within a 2D plane [Fig. 3(b) and Movie S2, Supplementary Information]. It is worth noting that the range of the rotation angle can be extended by enlarging the aspect ratio (w/h) of the light-activated film PG (Fig. S6, Supplementary Information) and expanding the area of the PG. Similar to 1D diffraction angle tuning, we reveal that wide spectral range of the incident wavelengths induces comparable 2D beam steering behaviors, as evidenced in Figs. 3(b) and 3(c), thereby providing ample flexibility in optical element design and application. Additionally, the clockwise rotation

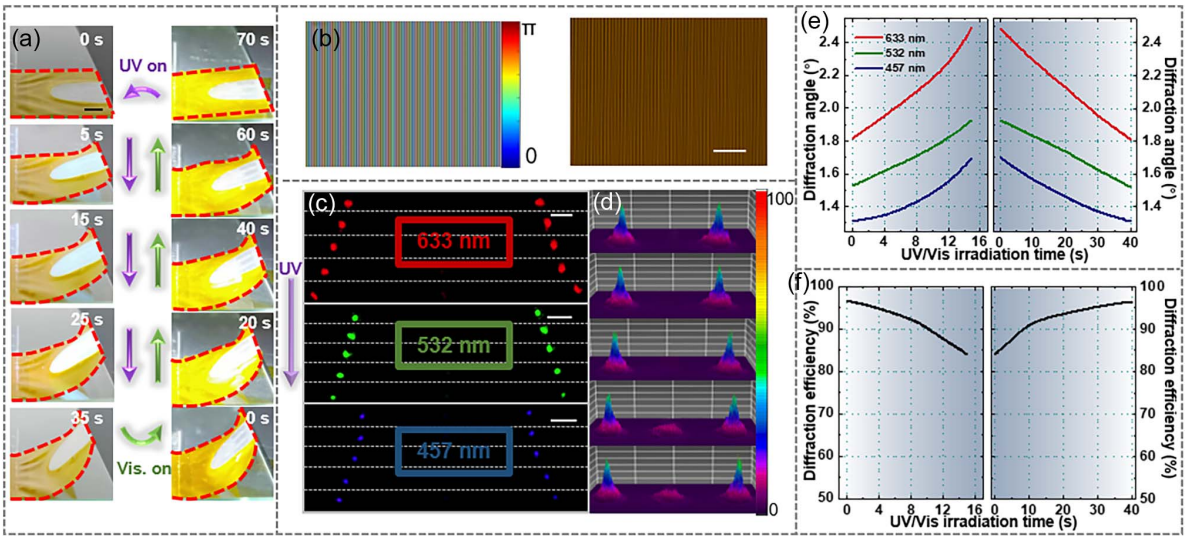

Fig. 2. Characterization of the 20-μm period light-activated film PG with 1D beam steering. (a) The deformation and recovery of the light-activated film PG under sequential UV light (365 nm, 10 mW·cm^{-2}) and visible light (500 nm, 20 mW·cm^{-2}) irradiation. The red dotted line outlines the deformation. The scale bar is 5 mm. (b) Phase distribution (left) and microscopy texture (right) of the 20-μm period PG. The scale bar is 200 μm. (c) Images of the ±1st order diffraction spots migrating in the 1D direction with UV light irradiation. From top to bottom, the UV light is irradiated at 0, 4, 8, 12, and 15 s. The incident light is linearly polarized with wavelengths of 633, 532, and 457 nm, respectively. The diffraction spots are captured at 70 cm. The scale bar is 5 mm. (d) Images of intensity distribution during the ±1st order diffraction spots migrating in the 1D direction. (e) Curve of the diffraction angle with UV/Vis irradiation time. (f) Curve of the diffraction efficiency with UV/Vis irradiation time.

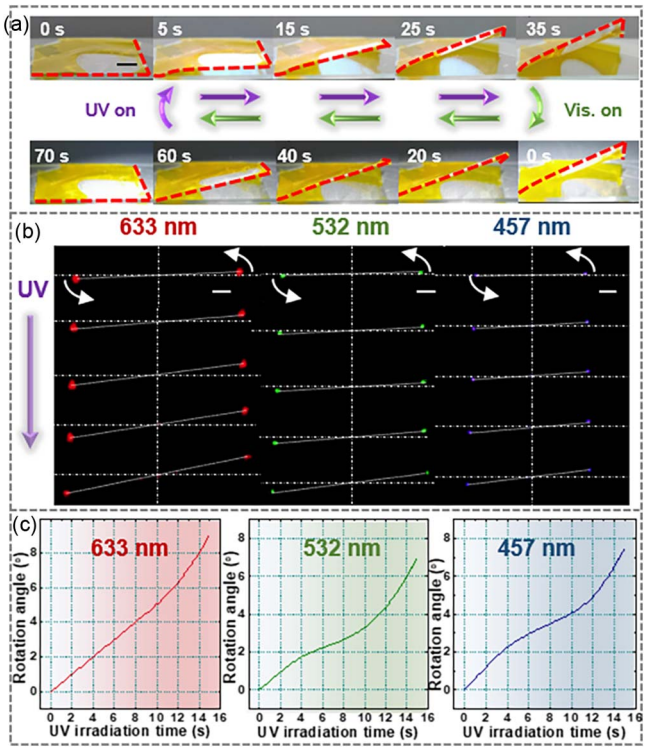

Fig. 3. Characterization of the 20-μm period light-activated film PG with 2D beam steering. (a) The deformation and recovery of the light-activated film PG under sequential UV light (365 nm, 10 mW·cm^{-2}) and visible light (500 nm, 20 mW·cm^{-2}) irradiation. The red dotted line outlines the deformation. The scale bar is 5 mm. (b) Images of the ±1st order diffraction spots rotating in the 2D plane with UV light irradiation. From top to bottom, the UV light is irradiated at 0, 4, 8, 12, and 15 s. The incident light is linearly polarized with wavelengths of 633, 532, and 457 nm, respectively. The diffraction spots are captured at 70 cm. The scale bar is 5 mm. (c) Curve of the 2D rotation angle of the ±1st order diffraction spot with UV irradiation time at incident wavelengths of 633, 532, and 457 nm, respectively.

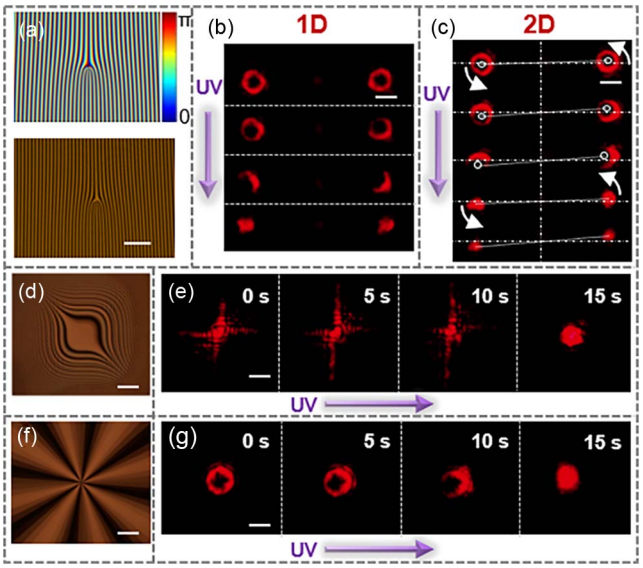

Fig. 4. Characterization of the light-activated film FPG, Airy mask, and q-plate with optical field modulations. (a) Phase distribution (top) and microscopy texture (down) of the light-activated film FPG with the period of 50 μm and the topological charge of +2. The scale bar is 200 μm. (b) Images of the ±1st diffracted order switching between vortex light and Gaussian light under UV light (365 nm, 10 mW·cm^{-2}) irradiation, based on the *x*-axis bending light-activated film FPG. From top to bottom, the UV light is irradiated at 0, 5, 10, and 15 s. The scale bar is 3 mm. (c) Images of the ±1st diffracted order switching between vortex light and Gaussian light under UV light (365 nm, 10 mW·cm^{-2}) irradiation, based on the diagonal bending light-activated film FPG. From top to bottom, the UV light is irradiated at 0, 4, 8, 12, and 15 s. The scale bar is 3 mm. (d) Microscopy texture of the Airy mask whose geometric phase distribution follows $\beta(x, y) = a(x^3 + y^3)$ in the *x*–*y* plane, where *a* is 4.05×10^{-7}. The scale bar is 200 μm. (e) Images of the switching between the Airy beam and Gaussian light with UV light (365 nm, 10 mW·cm^{-2}) irradiation based on the *x*-axis bending light-activated film Airy mask. The scale bar is 3 mm. (f) Microscopy texture of the q-plate with the topological charge of +4. The scale bar is 200 μm. (g) Images of the switching between the vortex light and Gaussian light with UV light (365 nm, 10 mW·cm^{-2}) irradiation based on the *x*-axis bending light-activated film q-plate. The scale bar is 3 mm. The incident light is linearly polarized with a wavelength of 633 nm. All diffraction spots are captured at 70 cm.

of the 2D beam steering is accomplished by adjusting the position of the PG on the light-activated LCP film (Fig. S7, Supplementary Information). Moreover, we demonstrate that altering the PG periods allows for different beam steering ranges, offering tailored solutions to meet specific application requirements (Figs. S8 and S9, Supplementary Information). Therefore, the high diffraction efficiency light-activated film PG with the capability for diffraction spots with 1D migration and 2D rotation, facilitates the integration and intelligence of advanced optical systems and can be used as a promising candidate for applications in projection displays, laser printers, and other optical systems.

Furthermore, various types of FDOEs boasting diversified optical field modulation capabilities are also demonstrated. As shown in Fig. 4(a), a fork polarization grating (FPG) with a period of 50 μm and a topological charge of +2 is designed to realize the structured optical field modulation. Incident light passing through the FPG is converted into vortex light with opposite topological charges at the ±1st diffraction order, showing doughnut-shaped spots on the screen (Fig. S10, Supplementary Information). Reversible switching between vortex and Gaussian lights is demonstrated both in the light-activated FPG bending along the *x*-axis or the diagonal direction under UV irradiation, accompanied by the migration in the 1D direction and the rotation in the 2D plane of the vortex optical singularities [Figs. 4(b) and 4(c)]. Additionally, we reveal that the 1D and 2D structured optical field modulation behaviors remain consistent across various incident light wavelengths (Fig. S11, Supplementary Information), as well as for varying the topological charges and the periods of the light-activated film FPG (Figs. S12 and S13, Supplementary Information), offering significant flexibility in the DOE design and fabrication. Thus, the proposed light-activated film FPGs featuring both 1D

and 2D dynamic and reversible structured optical modulation functions open up new avenues for the expansive realm of applications of light-activated FDOEs. The light-activated film Airy mask and q-plate are also investigated to further emphasize the universality in the optical field modulation of the light-activated FDOEs [Figs. 4(d) and 4(f)]. Notably, only the reversible switching of the Airy beam and single vortex light with Gaussian light happens, without the migration and rotation of the diffraction spots because both the Airy mask and the q-plate directly convert the incident light into an Airy beam or a vortex light without modulating the light propagation direction, as shown in Figs. 4(e) and 4(g). As exhibited, various types of FDOEs with the reversible switching between structured light and Gaussian light are easily achieved, heralding a new era characterized by the integration, intelligence, and miniaturization of optical systems.

To assess the practicability of the light-activated FDOEs, a series of performance tests, encompassing fatigue resistance, temperature stability, and solvent resistance, are implemented. Employing identical preparation procedures across all FDOE types ensures uniformity in performance evaluation. As a representative example, the 20 μm-period light-activated film PG is selected for detailed analysis. Robust fatigue resistance stands as a primary consideration for the practical application of the FDOEs. As illustrated in Fig. 5(a), even after undergoing 20 cycles of alternating UV and visible light irradiation, the light-activated film PG maintains its high diffraction efficiency and diffraction angle tunable range, proving its remarkable fatigue resistance. In addition, the light-activated film PG demonstrates adaptability to various solvent conditions, maintaining excellent optical performance even after a 4-h immersion in different solvent environments, such as water, alcohol, and n-hexane, as evidenced by the consistency in the initial diffraction efficiency and final diffraction angle, thus providing more application environments for the FDOEs [Fig. 5(b)]. Furthermore, temperature has been proved to barely impact the optical performance of the light-activated film PG. As shown in Fig. 5(c), the initial diffraction efficiency and the final diffraction angle remain identical after standing at both high (100°C) and low (−20°C) temperatures, facilitating the FDOEs application in extreme environments. Therefore, the light-activated FDOEs with robust fatigue resistance, excellent solvent resistance, and outstanding temperature stability, highlight their substantial potential in multifunctional applications including projection displays, laser printers, and light detection and ranging systems.

3. Conclusion

In conclusion, a novel approach for fabricating flexible, compact, and tunable light-activated FDOEs has been proposed by incorporating the LC geometry phase-based film DOE with the custom-designed light-activated LCP film, which has equipped the capability of 1D and 2D continuous and reversible beam steering, as well as dynamic switching between structure light and Gaussian light. To demonstrate the versatility of this method, four types of light-activated FDOEs have been mentioned. First, by designing the LC mesogens arrangement in the light-activated LCP film, a light-activated film PG has exhibited the migration in the 1D direction and the rotation in the 2D plane of ±1st order diffraction spots with the UV/Vis light irradiation, while maintaining high diffraction efficiency. Additionally, a light-activated film FPG has enabled the reversible switching between vortex light and Gaussian light under UV/Vis light irradiation. Moreover, the light-activated film Airy mask and the q-plate have exhibited reversible switching

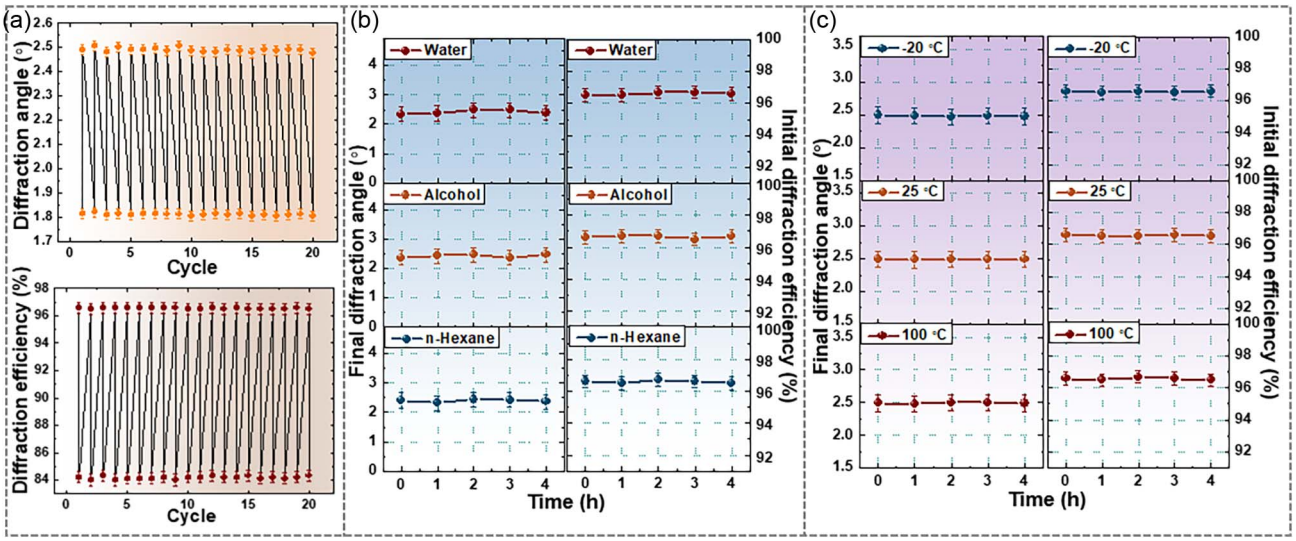

Fig. 5. Performance tests of the light-activated FDOE. (a) Fatigue resistance of the FDOE upon irradiations of UV light and visible light alternatively for 20 cycles. (b) Curve of the final diffraction angle (left) and initial diffraction efficiency (right) over time by immersing the FDOE in water, alcohol, and n-hexane. (c) Curve of the final diffraction angle (left) and initial diffraction efficiency (right) over time of the FDOE after standing at room temperature (25°C), high temperature (100°C), and low temperature (−20°C), respectively.

of the Airy beam or vortex light and Gaussian light. Noteworthy, the versatility of the light-activated FDOEs has extended to accommodating a broadband spectral range of incident light wavelengths through the meticulous design of the light-activated film, further proving the practicability and adaptability of the light-activated FDOEs. Furthermore, to ensure the reliability of the proposed light-activated FDOEs, comprehensive performance tests, including fatigue resistance, temperature stability, and solvent resistance have been conducted, affirming their suitability for diverse application environments. As optical systems advance toward greater intellectualization, weight reduction, and miniaturization, the demonstrated versatility and robustness of these flexible, compact, and tunable FDOEs could stimulate fresh momentum toward advanced optical applications, with promising prospects in fields such as integrated optical systems, intelligent optical devices, and flexible optics.

4. Experimental Section

The preparation process of the light-driven FDOEs was described in detail in Sec. S1 of the Supplementary Information. Microscopy textures were observed by a polarized optical microscope (LVPOL 100, Nikon) and recorded by a CCD camera (DS-U3, Nikon) under crossed linear polarizers. The 633, 532, and 457 nm lasers (Changchun New Industry, China) were utilized as light sources in our optical system. The pictures of macroscopic film deformation and the diffraction spot variations were captured by a digital camera (EOS 70D, Canon, Japan). The intensity distribution of the diffraction spots was detected and simultaneously analyzed by a CCD beam profiler system (SP620U, Spiricon). The diffraction efficiency was detected by an optical power meter (Thorlabs, America). The fatigue resistance was obtained by irradiating in sequence with UV light (365 nm, $10\,\mathrm{mW}\cdot\mathrm{cm}^{-2}$) and visible light (500 nm, $20\,\mathrm{mW}\cdot\mathrm{cm}^{-2}$) for 20 cycles. To determine the solvent resistance, the light-activated FDOE was immersed in water, ethanol (from Macklin), and n-hexane (from General-Reagent) for 4 h and recorded the initial diffraction efficiency and the final diffraction angle every 1 h. The temperature stability was assessed by keeping the light-activated FDOE at room temperature (25°C), high temperature (100°C), and low temperature (−20°C) for 4 h and recording the initial diffraction efficiency and the final diffraction angle every 1 h.

Acknowledgements

This work was supported by the National Key Research and Development Program of China (No. 2022YFA1203700), the National Natural Science Foundation of China (Nos. 62275081, 62035008, and 22305079), the Innovation Program of Shanghai Municipal Education Commission, Scientific Committee of Shanghai (No. 2021-01-07-00-02-E00107), the "Shuguang Program" of Shanghai Education Development Foundation, the Shanghai Municipal Education Commission (No. 21SG29), the Shanghai Sailing Program (No. 23YF1409000), the Fellowship of China National Postdoctoral Program for Innovative Talents (No. BX20230125), and the Postdoctoral Fellowship Program of CPSF (No. GZB20240218).

References

1. A. Ryabchun and A. Bobrovsky, "Cholesteric liquid crystal materials for tunable diffractive optics," Adv. Opt. Mater. **6**, 1800335 (2018).
2. M. Mitov, "Cholesteric liquid crystals with a broad light reflection band," Adv. Mater. **24**, 6260 (2012).
3. Y.-H. Zhang, S.-J. Liu, P. Chen, *et al.*, "Logical rotation of non-separable states via uniformly self-assembled chiral superstructures," Nat. Commun. **15**, 1108 (2024).
4. S. J. Liu, L. Zhu, Y. H. Zhang, *et al.*, "Bi-chiral nanostructures featuring dynamic optical rotatory dispersion for polychromatic light multiplexing," Adv. Mater. **35**, 2301714 (2023).
5. N. Yu and F. Capasso, "Flat optics with designer metasurfaces," Nat. Mater. **13**, 139 (2014).
6. L. Chen, J. Liu, M. Cheng, *et al.*, "Light-driven phase transition of diffractive optical elements based on liquid crystal elastomers," Opt. Express **32**, 12528 (2024).
7. L. Stern, D. G. Bopp, S. A. Schima, *et al.*, "Chip-scale atomic diffractive optical elements," Nat. Commun. **10**, 3156 (2019).
8. G. I. Greisukh, E. G. Ezhov, I. A. Levin, *et al.*, "Diffractive elements in the optical system: successes, challenges, and solutions," Radiophys. Quantum. El **57**, 610 (2015).
9. S. L. Oscurato, F. Reda, M. Salvatore, *et al.*, "Shapeshifting diffractive optical devices," Laser Photonics Rev. **16**, 2100514 (2022).
10. S. Schauer, T. Meier, M. Reinhard, *et al.*, "Tunable diffractive optical elements based on shape-memory polymers fabricated via hot embossing," ACS Appl. Mater. **8**, 9423 (2016).
11. G. Zhou, F. E. H. Tay, and F. S. Chau, "Design of the diffractive optical elements for synthetic spectra," Opt. Express **11**, 1392 (2003).
12. F. Yong-Qi, N. K. A. Bryan, and O. N. Shing, "Diffractive optical elements with continuous relief fabricated by focused ion beam for monomode fiber coupling," Opt. Express **7**, 141 (2000).
13. L. L. Doskolovich, A. A. Mingazov, E. V. Byzov, *et al.*, "Hybrid design of diffractive optical elements for optical beam shaping," Opt. Express **29**, 31875 (2021).
14. T. Zhou, Q. Du, T. Sano, *et al.*, "Two-dimensional combination of eight ultrashort pulsed beams using a diffractive optic pair," Opt. Lett. **43**, 3269 (2018).
15. Z. Luo, Y. Li, J. Semmen, *et al.*, "Achromatic diffractive liquid-crystal optics for virtual reality displays," Light Sci. Appl. **12**, 230 (2023).
16. N. V. Tabiryan, D. E. Roberts, Z. Liao, *et al.*, "Advances in transparent planar optics: enabling large aperture, ultrathin lenses," Adv. Opt. Mater. **9**, 2001692 (2021).
17. P. Chen, B.-Y. Wei, W. Hu, *et al.*, "Liquid-crystal-mediated geometric phase: from transmissive to broadband reflective planar optics," Adv. Mater. **32**, 1903665 (2020).
18. P. Sun, B. Liu, Y. Wang, *et al.*, "Ultrabroadband multichannel vector vortex beams with versatile electrically induced functionality," Laser Photonics Rev. **17**, 2300098 (2023).
19. C.-J. Yun and J.-K. Song, "Functional films using reactive mesogens for display applications," J. Inform. Display **18**, 119 (2017).
20. X. Pang, J. A. Lv, C. Zhu, *et al.*, "Photodeformable azobenzene-containing liquid crystal polymers and soft actuators," Adv. Mater. **31**, 1904224 (2019).
21. J. Chen, A. S. Johnson, J. Weber, *et al.*, "Programmable light-driven liquid crystal elastomer kirigami with controlled molecular orientations," Adv. Intell. Syst. **4**, 2100233 (2022).
22. K. Mehta, A. R. Peeketi, L. Liu, *et al.*, "Design and applications of light responsive liquid crystal polymer thin films," Appl. Phys. Rev. **7**, 041306 (2020).
23. Y. Wang, J. Liu, and S. Yang, "Multi-functional liquid crystal elastomer composites," Appl. Phys. Rev. **9**, 011301 (2022).
24. A. Kudreyko, V. Chigrinov, G. Hegde, *et al.*, "Photoaligned liquid crystalline structures for photonic applications," Crystals **13**, 965 (2023).
25. Z.-X. Shen, M.-J. Tang, P. Chen, *et al.*, "Planar terahertz photonics mediated by liquid crystal polymers," Adv. Opt. Mater. **8**, 1902124 (2020).

26. Y. Li, Y. Liu, and D. Luo, "Polarization dependent light-driven liquid crystal elastomer actuators based on photothermal effect," Adv. Opt. Mater. **9**, 2001861 (2020).
27. Y. Huang, H. K. Bisoyi, S. Huang, *et al.*, "Bioinspired synergistic photochromic luminescence and programmable liquid crystal actuators," Angew. Chem. Int. Ed. Engl. **60**, 11247 (2021).
28. W. Wei, Z. Zhang, J. Wei, *et al.*, "Phototriggered selective actuation and self-oscillating in dual-phase liquid crystal photonic actuators," Adv. Opt. Mater. **6**, 1800131 (2018).
29. L. Tan, A. C. Davis, and D. J. Cappelleri, "Smart polymers for microscale machines," Adv. Funct. Mater. **31**, 2007125 (2020).
30. R. Zheng, L. Ma, W. Feng, *et al.*, "Autonomous self-sustained liquid crystal actuators enabling active photonic applications," Adv. Funct. Mater. **33**, 2301142 (2023).
31. O. M. Wani, H. Zeng, P. Wasylczyk, *et al.*, "Programming photoresponse in liquid crystal polymer actuators with laser projector," Adv. Opt. Mater. **6**, 1700949 (2018).
32. Y. Chen, C. Valenzuela, X. Zhang, *et al.*, "Light-driven dandelion-inspired microfliers," Nat. Commun. **14**, 3036 (2023).
33. M. Yang, Y. Xu, X. Zhang, *et al.*, "Bioinspired phototropic MXene-reinforced soft tubular actuators for omnidirectional light-tracking and adaptive photovoltaics," Adv. Funct. Mater. **32**, 2201884 (2022).
34. D. Wu, Y. Zhang, H. Yang, *et al.*, "Scalable functionalized liquid crystal elastomer fiber soft actuators with multi-stimulus responses and photoelectric conversion," Mater. Horiz. **10**, 2587 (2023).
35. Z. Zhang, X. Yang, Y. Zhao, *et al.*, "Liquid crystal materials for biomedical applications," Adv. Mater. **35**, 2300220 (2023).
36. H. Zeng, O. M. Wani, P. Wasylczyk, *et al.*, "Self-regulating iris based on light-actuated liquid crystal elastomer," Adv. Mater. **29**, 17001814 (2017).
37. B. Jin, J. Liu, Y. Shi, *et al.*, "Solvent-assisted 4D programming and reprogramming of liquid crystalline organogels," Adv. Mater. **34**, 2107855 (2022).
38. W. Gu, J. Wei, and Y. Yu, "Thermo- and photo-driven soft actuators based on crosslinked liquid crystalline polymers," Chin. Phys. B **25**, 096103 (2016).
39. K. Kim, C. Lee, and D. K. Yoon, "Patterned hydrophobic liquid crystalline fibers fabricated from defect arrays of reactive mesogens via electric field modulation," ACS Appl. Mater. **15**, 8387 (2023).
40. Y. Yang, X. Zhang, C. Valenzuela, *et al.*, "High-throughput printing of customized structural-color graphics with circularly polarized reflection and mechanochromic response," Matter **7**, 2091 (2024).
41. X. Zhang, L. Li, Y. Chen, *et al.*, "Mechanically tunable circularly polarized luminescence of liquid crystal-templated chiral perovskite quantum dots," Angew. Chem. Int. Ed. **63**, e202404202 (2024).